PERMEATION CHARACTERISTICS OF GRAMICIDIN CONFORMERS

DAVID BUSATH AND GABOR SZABO
Department of Physiology and Biophysics, University of Texas Medical Branch, Galveston, Texas 77550

ABSTRACT To investigate the molecular origin of decreased conductance in variant gramicidin channels, we examined the current-voltage (IV) characteristics of single Val[1]-gramicidin A channels. Unlike standard channels, all variant channels showed pronounced rectification even though bathing solutions were symmetrical. Moreover, channels of lower conductance consistently showed more pronounced rectification. Analysis within the framework of a three-barrier, two-site, single-filing model indicates that the shape of the variant channel IVs could be best explained by an increase in binding affinity near one of the two channel entrances. This conclusion was further tested by characterizing single channel IVs in bi-ionic solutions having different cationic species at each channel entrance. In Cs/Na bi-ionic solutions, reversal potentials of variant channels often differed by a small but significant amount from those of standard channels. When a membrane potential was applied, the ionic currents tended to be reduced more when flowing from the Na^+ side than the Cs^+ side. These observations support the conclusion that variant channels have increased binding affinity at one end of the channel. Furthermore, H^+ currents were increased while Ag^+ currents were unaltered for most variant channels exhibiting decreased Na^+ or Cs^+ currents. The increased H^+ conductance argues against long-range coulombic forces as the basis for decreased Na^+ or Cs^+ conductance while the normal Ag^+ conductance suggests that the binding site field strength increases by a change in carbonyl geometry at the channel entrance.

INTRODUCTION

Gramicidin A was previously shown to form a spectrum of variant "mini" channels which differ from the predominant standard channels in their conductance but not in their overall molecular structure (Busath and Szabo, 1987). Since minis form a roughly continuous spectrum of conductance states, it is reasonable to suppose that some localized molecular change, varying in degree over a continuous range, underlies these conductance changes. We develop here an "ionometric" method to elucidate the origin of these molecular changes by analyzing their effects on the energetics of ion permeation through single, ion-conductive channels.

Mini channels could not be physically isolated or purified and each one appears to be a unique, metastable conformational variant (Busath and Szabo, 1988). Methods that probe a population of molecules, such as spectroscopic (e.g., Monoi and Uedaira, 1979) or tracer flux measurements (e.g., Shagina, Grinfeldt and Lev, 1978), would be poorly suited for the study of these molecular variants. Single-channel current measurements, in contrast, allow one to probe individual molecules by measuring the flow of ions through them.

We have implemented the ionometric method of structural analysis by determining current-voltage relationships for individual standard and variant channels in the presence of various permeant cations. By comparing the observed spectrum of current-voltage (IV) characteristics with the theoretically predicted spectrum of IV characteristics obtained using the two barrier, three-site single-file model (Urban and Hladky, 1979), it has proven feasible to identify the location and nature of the molecular changes that generate mini channels. A similar ionometric approach should be particularly well suited to study conformational variations in biological channels whose molecular structures are presently not well understood.

METHODS

The experimental apparatus and procedures were described in the preceeding paper (Busath and Szabo, 1988). Single-channel current-voltage relationships (IVs) were measured as follows. A 0.5 Hz triangular voltage signal was applied to the membrane by directly connecting the 50-ohm output of a wave form generator (model 5600; Krohn-Hite Corp., Avon, MA) to the Ag-AgCl electrode in the front chamber while the rear chamber was held at virtual ground by a low noise current amplifier. Channels lasting at least 5–6 cycles and bracketed by several cycles having no channels (baseline), were analyzed by averaging single-channel currents in 0.5 mV-wide membrane potential bins and subtracting the baseline current binwise. The standard error (SE_i) for the measurements of the current, I^o, in each bin was estimated and used to determine the goodness-of-fit of the theoretical predictions. The observed average current in each bin, I_i^o was compared with the predictions of the model, I_i^t and a weighted, reduced chi square parameter was calculated by summing over all the voltage bins containing measurements:

$$X^2_{red} = \frac{1}{N_d - N_p} \sum_i (I_i^o - I_i^t)^2 / SE_i^2, \quad (1)$$

where N_d is the number of voltage bins for which an average single

Dr. Busath's present address is Section of Physiology and Biophysics, Box G, Brown University, Providence, RI 02912

channel current has been observed and N_p is the number of parameters in the model. An acceptable fit will yield $X^2_{red} < 2$ (Bevington, 1969; see also Urban and Hladky, 1979).

The model predictions, I_i^1 were calculated using a rate theory model similar to those described by others (Woodbury, 1971; Sandblom, Eisenman and Neher, 1977; Hille and Schwarz, 1978; Urban and Hladky, 1979; Begenisich and Cahalan, 1980; Urry et al., 1980). We used the three-barrier two-site version because, although it was sufficiently detailed to provide a good fit of single-channel IVs, it was simple enough to allow the formulation of general conclusions.

Curve-fitting was done only for the single permeant-species case. The channel was considered to assume any of four occupancy states: doubly occupied, occupied on either side (entry or exit), or empty. Conversions between the states follow first order kinetics. The rate constant, k, for occupancy state interconversion is interpreted according to the Eyring formalism (Eyring et al., 1949):

$$k = q\, kT/h \exp\,[-(G_B - G_W)/RT]. \qquad (2)$$

The transmission coefficient, q, is taken to be unity; G_W is the free energy of an ion in a well and G_B is the free energy of the adjacent barrier; k, T, h, and R are respectively Boltzmann's constant, absolute temperature, Planck's constant, and the gas constant. The effective positions of the peaks and wells determine an increment of energy $\sigma FV/RT$ added to G_B and G_W, when a membrane potential, V, is applied to the front chamber, where σ is the fraction of the distance through the electric field of the barrier or well measured from the back chamber which is maintained at virtual ground. F is Faraday's constant. The rates of entry and exit of a second ion are allowed to be different from those of the first ion by including additional energy terms, ΔG_B and ΔG_W, which are added to the external barrier and well respectively, when the opposite site is occupied. The channel current (in amps, front to back) is given for monovalent cations by:

$$I = e\,(k_{12}P_1 - k_{21}\,P_2), \qquad (3)$$

where e is the electronic charge in coulombs, k_{12} and k_{21} are rate constants for translocation from site 1 to 2 and vice versa, and P_1 and P_2 are the occupancy probabilities for sites 1 and 2 computed using the matrix-inversion method (Begenisich and Cahalan, 1980).

In the modeling process, the rate constants were varied by changes in the heights and positions of the entry and exit barrier, the height of the central barrier, the depths and positions of the two wells, and the amounts of the additional energy terms which relate to double occupancy, ΔG_B and ΔG_W. The location of the barriers and wells for the doubly-occupied pore were not varied for three reasons. First, symmetric relocations of the binding sites (as might be intuitively expected to occur for two ions each repelled by the other's electrostatic potential or image potential) are disallowed by microscopic reversibility (Urban and Hladky, 1979, see Eqs. 15 and 16). Second, asymmetric relocations of the binding sites (that is, shifts of both wells to the right or to the left), although allowed by microscopic reversibility, were judged physically unreasonable. Third, displacement of the barrier to second ion entry/exit, while satisfying microscopic reversibility, was disallowed both in order to reduce the degrees of freedom in the model and because this would only have secondary effects on the resulting IVs.

Barrier parameters for standard Val[1]-gramicidin A channels were determined by simultaneously fitting standard channel IVs obtained in three different concentrations of KCl, 3.0, 1.0, and 0.1 M. The standard channel barrier patterns were constrained to be symmetric about the center of the membrane. The barrier positions were chosen initially to be 0.05 of the membrane field from the channel entrance (Eisenman and Sandblom, 1983). The binding site was started at 0.14 of the field from the entrance (Andersen and Procopio, 1980). The well-depth was chosen to be fairly shallow. This is similar to FIT I in Urban et al., 1978; (see also McBride, 1981). The curve fitting routine was then allowed to seek the best entry barrier and central barrier heights and later to vary all the parameters to optimize the simultaneous fit for the three IVs. A similar procedure was carried out with various other starting points including several runs with randomly chosen starting parameters and one fit with deep wells (-6 RT) which was similar to FIT II of Urban et al., 1978 and the fit in Urban et al., 1980. The binding site affinity was poorly constrained by the data because, for any chosen binding affinity, the IVs could be fairly well fit provided that the second ion binding affinity was adjusted to $\sim 1\ M^{-1}$.

Variant channel IVs were fit using the standard channel parameters as starting estimates. All but one, two, or three of the parameters being examined were held fixed at the standard channel values. In some cases, we used randomly chosen starting estimates for the varied parameters to search for alternative local minima in the χ^2 surface. For the one and two parameter fits, other minima were few and were easily rejected both by visual and statistical criteria. In some cases the alternative minimum gave a fit superior to that obtained using the standard parameters as a starting point and was therefore preferred.

For bi-ionic measurements, after filling both of the chambers with one solution, the solution in the front chamber was replaced by a new solution with care to avoid mixing with the contents of rear compartment. A bilayer was then formed. In most cases the consequences of any mixing which may have occurred before forming the bilayer dissipated rapidly; the single-channel reversal potentials for standard channels immediately assumed a constant value. Control experiments using 1 M NaCl on one side, 0.25 M NaCl on the other side yielded reversal potentials of 25.7 mV ($\pm$ 1.4 mV, S.D., $n = 36$) for standard channels and 24.1 mV ($\pm$ 3.1 mV, S.D., $n = 16$) for mini channels. They are less than the predicted Nernst potential for Na (assuming mean ionic activity coefficients from Robinson and Stokes, 1965), 32.3 mV. The discrepancy is expected due to the channel streaming potential and the effects of osmosis on unstirred layers, both arising from the osmotic gradient (Levitt et al., 1978; Rosenberg and Finkelstein, 1978). In HCl solutions, Levitt et al. (1978) found no streaming potential, consistent with no coupling between proton and water transport in the channel as would be predicted for a Grotthuss H^+ conductance mechanism. Likewise, with 0.01 HCl on one side of the membrane and 0.10 HCl on the other, we measured the reversal potential to be 53.9 mV ($\pm$ 1.3 mV, S.D., $n = 35$) which can be compared with the predicted activity-corrected Nernst potential for H^+, 54.3 mV. These reversal potentials indicate that both standard and mini channels are cation selective and that the cation concentration gradient is rapidly established.

RESULTS

The current-voltage relationship for a channel was easily distinguished from that of the lipid bilayer. This is evident in the current trace of Fig. 1 where a channel opens in the sixth cycle and then closes after six cycles. In most cases single-channel IVs remained unaltered throughout the lifetime of the channel. In a few cases where channels were

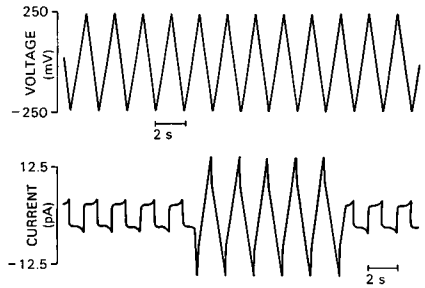

FIGURE 1 Time series of applied potential (*top*) and membrane current (*bottom*) during the occurrence of one standard gramicidin A channel. The raw data, sampled at 500 Hz, are plotted with the points connected. 1 M KCl, 100 Hz low-pass filter.

observed to change conductance during their lifetime, the IVs changed abruptly between two well defined, stable shapes.

Symmetric Solutions

The IVs for standard channels in 3.0, 1.0, and 0.1 M KCl are shown in Fig. 2. The data are shown as error bars whose size reflect the current noise. The solid curves display the predictions of the symmetric three-barrier, two-site model using the optimal parameters listed and defined in Table I. The inset of Fig. 2 shows a schematic representation of this standard channel barrier pattern. With an ion occupying the left-hand binding site the change in the effective barrier pattern for a second ion entering from the right is represented by the dashed curve. The IVs of standard channels are saturating at low concentrations, linear at moderate concentrations, and superlinear at high concentrations. This is consistent with previous observations using multi-channel or single-channel studies (Hladky and Haydon, 1972; Andersen, 1983; Eisenman and Sandblom, 1983). In general, standard channel IVs were symmetric about the origin and superimposed upon each other within the noise band.

A small deviation of the fit from the 1.0 M data is evident in Fig. 2. It is sufficient to cause the x^2_{red} to be considerably higher (16.7) than the statistically acceptable value (~2). When fitting the three IVs simultaneously, no single sets of parameters could be found that would entirely eliminate this weakness indicating that the three-barrier, two-site model is too simple to precisely describe K^+ permeation of gramicidin. Inadequacies of the model become more apparent at 0.01 M KCl, where the predicted currents are 40–50% lower than the observed currents (data not shown). More complicated models would undoubtedly provide a better fit to the standard channel IVs (Eisenman et al., 1978). Nevertheless we proceeded with the simple model with the idea that it would more clearly demonstrate the major energetic changes that cause lowered channel conductance.

TABLE I
STANDARD CHANNEL PARAMETERS

G_1, G_5	10.8 RT	entry barrier height
G_2, G_4	−1.39 RT	binding site depth
G_3	10.1 RT	central barrier height
$\alpha_1, 1-\alpha_5$	0.0605	entry barrier position in field
$\alpha_2, 1-\alpha_4$	0.154	binding site position
α_3	0.500	central barrier position
$\Delta G_1, \Delta G_5$	0.272 RT	increase in entry barrier height with the opposite site occupied
ΔG_2	0.907 RT	decrease in well depth during double occupancy

The curvature in mini channel IVs varies from channel to channel. Examination of many IVs from various experiments on different days failed to reveal any characteristic IV shape. Therefore, we chose for detailed analysis a group of channels which had conductances spanning the mini range and which seemed to represent the diversity of IV shapes as well. This group consisted of 23 minis obtained from a typical experiment. In all 23 cases, the individual sweeps for a given channel were identical in appearance. Thus the IV shape for a given channel is reproducible and stable. All 23 IVs rectified, even though the membrane and aqueous solutions were symmetrical. The ratio, R, was defined as I(+200 mV)/I(−200 mV). In the sample chosen, R was greater than unity for 10 channels, less than unity for 13. Minis and standards seemed to occur in

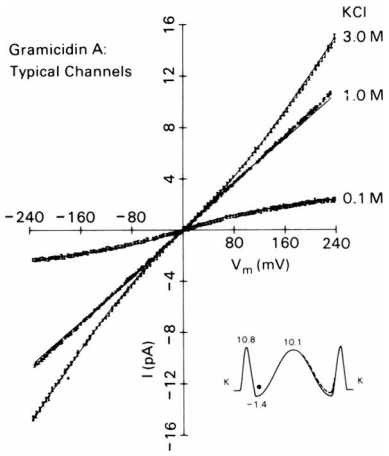

FIGURE 2 Current-voltage relations for representative standard channels measured in 3.0 M, 1.0 M, and 0.1 M KCl. Each bar represents ±2 S.E. from the mean of 3 to 5 observations in the voltage bin. The solid curves are the predictions of the kinetic model using the parameters for standard channels given in Table I. *Insert:* A diagramatic representation of the kinetic parameters interpreted as free energy barriers as described in the text. Only the heights and positions of extrema are used in the theory. The dashed curve represents the energy pattern for a second ion if the left-hand well is occupied. Upon occupancy by the second ion, the energy pattern for the left hand ion is modified in the same way, i.e., the pattern remains symmetrical. The free energies are given in multiples of RT for K^+ transport.

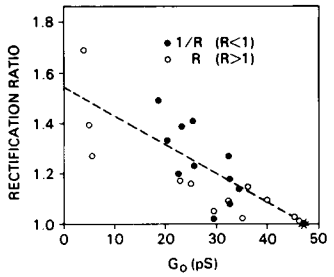

FIGURE 3 Mini channel rectification correlates negatively with channel conductance. The rectification ratio, R, is plotted against the channel IV slope conductance at 0 mV potential for channels having $R > 1$ (*open circles*) and the inverse of R for channels having $R < 1$ (*closed circles*). The mean value for the group of standard channels is represented by a single point (*filled sun*). The dashed line is a visual guide; it has no theoretical or statistical significance. 1 M KCl, $R = -I(+200\text{ mV})/I(-200\text{ mV})$. GMO Hex 50 mg/ml 23°C.

random order. The direction and degree of rectification for the minis varied from channel to channel. The degree of rectification for the minis varied from channel to channel. The degree of rectification appeared to correlate with the amount of conductance decrease, measured as the zero-current slope conductance. This is demonstrated in Fig. 3 where R or 1/R are plotted against zero-current conductance. The shapes of four of the mini channel IVs having zero current conductances of between 4 and 28 pS are illustrated in Fig. 4. The circles represent the average of currents from all sweeps for each channel.

We considered the possible causes of decreased conductance and asymmetry in mini channel IV curves. One simple approach is to examine the predictions of the Eyring rate theory model, changing the parameters of the three barrier, two-site model one by one. Increasing the entry or exit barrier and deepening the entry or exit well all decrease the channel conductance. In a nonsaturating channel deepening the entry or exit well would not be expected to affect the conductance (Eyring et al., 1949). However, in a gramicidin-type saturating channel, the occupancy increase caused by well-deepening is limited whereas the rate constant for ions leaving the channel site declines without limit resulting in a decreased channel conductance.

Asymmetric barrier pattern changes predict asymmetric IV relations. The sidedness of the asymmetry in the IVs follows a consistent pattern. The model predicts a greater reduction in channel current if the barrier adjacent to the positive side is raised than if the opposite barrier is raised. Thus, a channel with an abnormally high barrier oriented towards the front chamber would conduct less when the front chamber is held positive than when it is held negative, i.e., would have $R < 1$. On the other hand, the model predicts a lesser reduction in channel current if the well adjacent to the positive side is deepened than if the opposite well is deepened. Thus a channel with an abnormally high binding affinity oriented towards the rear chamber would conduct better when the rear chamber is held positive, i.e., would have $R < 1$. Finally, our model predicted that deepening a well would produce much greater asymmetry than would raising a barrier.

Because of these qualitative predictions, and because it is reasonable to suppose that similar kinds of molecular changes may occur at either side of the channel, we defined channel orientation according to the asymmetry observed.

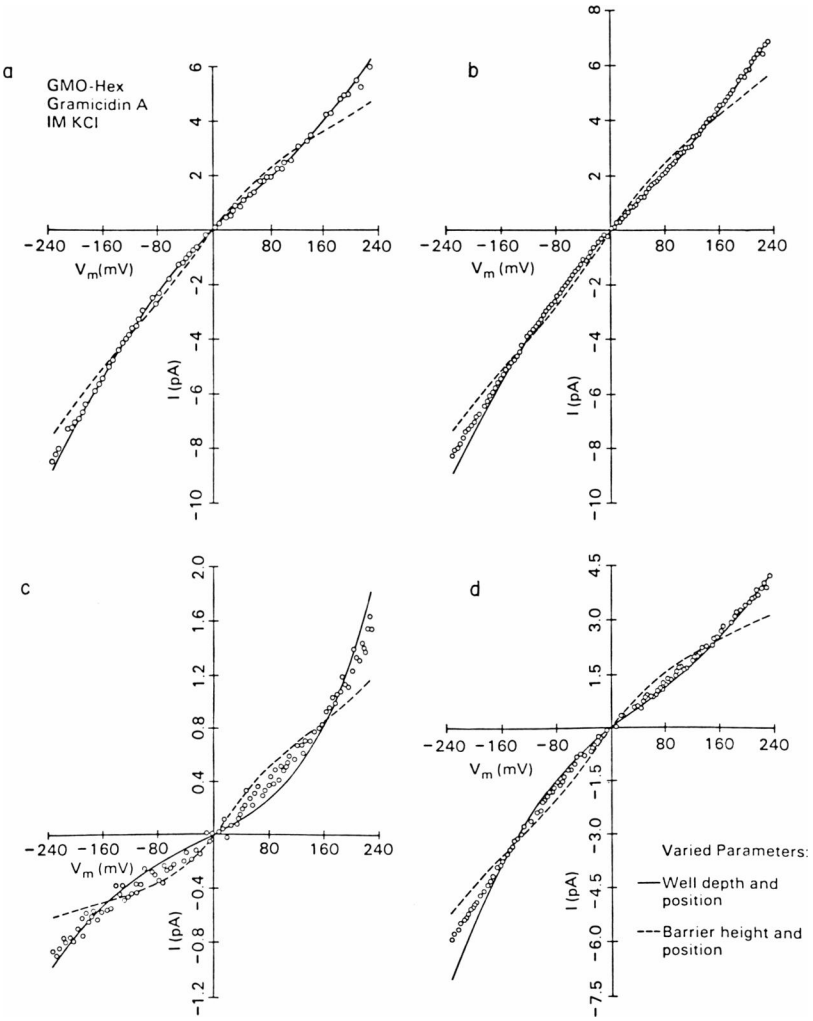

FIGURE 4 Current-voltage relations for four (out of 23) channels representing the range of observed channel conductance. As in Fig. 2, each point represents the mean of 2–5 observations for the voltage bin; error bars are not shown but are similar to those in Fig. 2. (*Solid curves*) Best fit of the model of Table I after allowing the *cis* well and its position (G_2 α_2) to vary. (*Dashed curve*) Best fit after allowing the *cis* barrier and its position (G_1 α_1) to vary. GMO Hex (50 mg/ml); 1 M KCl, 23°C. *a* DB24; *b* DB3T; *c* DB20B; *d* DB39.

For channels which conducted better for positive potentials applied to the front chamber (i.e., R > 1), we defined the side towards the front chamber as the *cis* side. For channels which conducted better for negative potentials applied to the front chamber (i.e., R < 1), we defined the side towards the rear chamber as the *cis* side. Using this convention, the barrier pattern was numbered from *cis* to *trans*.

We first fit the mini IVs with the standard channel model allowing only one parameter to vary. After finding the best fit for each channel, the x^2_{red}'s from all the channels were averaged to get an overall goodness of fit. Table II gives the average x^2_{red} and, as a measure of the variations from channel to channel, the SE (x^2_{red}). In general, a $x^2_{red} <$ 4 yielded a fit where the predicted IV passed through most error bars. Higher values of x^2_{red} resulted when noticeable deviations occurred. Values up to 60 or 70 were obtained when the predicted IV shape was qualitatively satisfying but with moderate deviations. Fits with values above 100 were obviously inadequate. Raising the *cis* barrier improved the average x^2_{red} from 3,443 (the value obtained using the standard channel parameters directly) to 122. Deepening the *cis* well had a similar effect, x^2_{red} was decreased to 168. Deepening the *trans* well, in contrast, yielded a much less effective fit. Although it reduced the conductance appropriately, it predicted rectification in the wrong direction so that the goodness of fit (x^2_{red} = 624) was much worse than for the *cis* well deepending. Raising the *trans* barrier, on the other hand, was nearly as successful as raising the *cis* barrier (x^2_{red} = 135 vs. 122) because barrier height increases result in very little rectification in both cases. In all four fits the zero current conductances roughly agreed with the observed values, but the IV shapes were grossly inadequate. We would consider these zero order fits.

Next we performed a second set of fits where either a barrier and its position or a well and its position were varied simultaneously. Two of these yielded satisfying first order predictions: x^2_{red} = 73 for the *cis* barrier fit and 17 for the *cis* well fit (see Table II). Examples of these two fits are plotted in Fig. 4. For each single channel IV, the dashed curve is the prediction of the best *cis* barrier (height and position) fit. Note that the conductance is approximately right for each fit and that the rectification is in the right direction, a first order fit. However, in each case the secondary inflections (d^2I/dV^2) are opposite to those in the data. We found this to be the case for all 23 channels under study. The solid curves show the predictions of the *cis* well (depth and position) fit. Unlike the *cis* barrier fit, the *cis* well fit yields not only the correct conductance and rectification, but also the correct directions for the secondary inflections, giving a satisfactory second order fit[1].

TABLE II

Parameter(s) varied		Goodness of fit
Cis barrier height	*G*1	122 ± 19
and position	*G*1, α1	73 ± 12
and entry well	*G*1, *G*2	50 ± 8
Cis well depth	*G*2	168 ± 24
and position	*G*2, α2	17 ± 5
and 2nd ion barrier	*G*2, Δ*G*5	30 ± 6
and central barrier	*G*2, *G*3	34 ± 8
Trans well depth	*G*4	624 ± 117
and position	*G*4, α4	34 ± 8
and 2nd ion barrier	*G*4, Δ*G*1	65 ± 10
and central barrier	*G*4, *G*3	120 ± 29
Trans barrier height	*G*5	135 ± 22
and position	*G*5, α5	76 ± 12
and entry well	*G*5, *G*4	89 ± 14

The difference in goodness of fit between the *cis* barrier fit and the *cis* well fit can be compared statistically using the traditional F test (Bevington, 1969). The ratio of the total x^2 from two different fits is F distributed with N degrees of freedom, where N is the total number of points fit. Between the *cis* well fit and the *cis* barrier fit, the ratio of total x^2 was 4.3 indicating that there is a low probability that the *cis* barrier fit is as good as the *cis* well fit ($P \ll 0.05$, $N > 2300$). This is more clearly demonstrated in Table III which shows x^2_{red} from the second order fits for each channel. The channels are listed in two groups in order of ascending conductance, G_0, calculated as the slope of the line fit by least squares to current points between −10 and +10 mV. The first group (DB39 to DB2Z) had $R < 1$; the second group (DB20B to DB2Q) had $R > 1$. Of the 23 IV's analyzed, 21 were best fit by the *cis* well (G_2, α_2) model. These considerations led us to conclude that a change in the *cis* well and its location can best account for the observed asymmetrical IV's of the mini channels.

Several other types of fits were performed also. The average of the x^2_{red}'s is given in Table II for each of several fits as well as the standard error of the average, which reflects the variation in the goodness of fit among the 23 channels considered. Three and four parameter fits were also explored (data not shown) with the general result that as long as a well is one of the varied parameters, the data are fit extremely well. However, because of the large amount of freedom in these fits, the data would not meaningfully constrain the parameters varied in the model.

The well-deepening required to fit the variant channels was proportional to the decrease in zero-current conductance. This is shown in Fig. 5 which plots, for each of the observed channels, the well-depth obtained from the

[1]Because uncertainties exist concerning the depth of the well in the standard channel model, we wished to acertain that this conclusion does not depend on the particular initial value of the well depth we chose. We therefore repeated the fit using an alternative standard channel parameter set which was derived using a well depth of $-6RT$. The results were the same as those displayed in Fig. 4. The inflections of the data were parallel to those in the data if the exit well was made deeper, but counter to the data if the entry barrier was raised.

TABLE III

Name	G_o	*Cis* barr.	*Cis* well	*Trans* well	*Trans* barr.
	PS	$G1, \alpha1$	$G2, \alpha2$	$G4, \alpha4$	$G5, \alpha5$
DB39	18.4	67	19	39	78
DB2VA	20.2	90	3	17	75
DB2VB	22.7	204	7	26	213
DB2G	23.0	166	11	47	181
DB2A	25.3	77	5	30	81
DB24	25.8	107	10	45	124
DB35B	29.3	46	43	43	45
DB2FA	32.2	96	3	13	101
DB2FB	32.4	67	4	32	69
DB3T	32.6	60	57	179	77
DB40A	34.2	36	5	25	40
DB40B	45.8	15	9	8	16
DB2Z	46.3	34	76	44	31
DB20B	3.9	8	4	5	7
DB2H	4.8	12	9	9	14
DB3R	5.4	16	6	7	13
DB28	23.0	73	3	8	73
DB20A	24.9	203	3	7	202
DB35A	29.9	31	69	95	31
DB3W	32.2	95	9	23	96
DB33	35.2	90	17	24	88
DB2X	36.2	53	14	49	53
DB2Q	39.9	29	2	13	30
Number of preferred fits:		1	21	1	0

(G_2, α_2) fit against the measured zero-current conductance. The solid line shows the calculated *cis* well deepening required to produce a given zero-current conductance. Clearly an increase in the binding affinity of one site, relative to the channel exterior, reduces channel conductance.

Asymmetric Solutions

To further test the theory that the well depth is increased on one side in minis, we measured single channel IVs in a variety of asymmetric solutions. In the experiments reported here, the solution in the front chamber was replaced with a solution of a different salt. The inset in Fig. 6 shows two single-channel IVs obtained when the front chamber solution is 1M NaCl and the rear chamber solution is 1 M CsCl. The IV of greater conductance is a standard channel. It conducts better at negative voltages (Cs^+ mediated current) than at positive voltages (Na^+ mediated current) consistent with gramicidin's greater permeability to Cs^+.

The mini channel in the inset of Fig. 6 has a decreased conductance and a slight positive shift in the zero-current potential. Other minis observed typically had little or no shift (0–6 mV) in reversal potential (data not shown). For the mini in Fig. 6, the reduction in conductance is more pronounced at positive voltages, i.e., when Na^+ is the predominant current carrier. Because of the complexity of the three-barrier, two-site model for two permeant ions, we

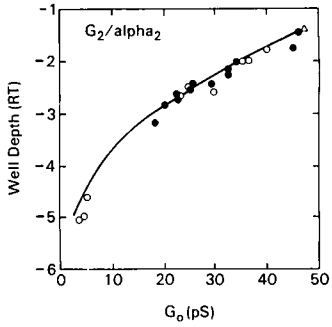

FIGURE 5 The optimal value of the *cis* well depth from the G_2, α_2 fit is plotted for each of the 23 mini channels against the slope conductance at zero mV (G_0) for the channel, obtained using a least squares fit to current points between −10 and +10 mV. The triangle represents the standard channels. The solid curve gives the zero-voltage slope conductance prediced by the model parameters from Table I but with G_2 (only) as an independent variable. Filled circles, R < 1; open circles, R > 1.

chose not to fit bi-ionic single-channel IVs. We discovered, however, that the three-barrier two-site model predicted a simple outcome if well-depths are changed differentially on one side of the channel. If a well for Na^+ is deepened more than the well for Cs^+, the model predicts that, for moderate applied potentials, the Na^+ mediated current will be decreased more than the Cs^+ mediated current produced by the same potential of opposite polarity. This rule proved to be independent of the side of the channel on which the

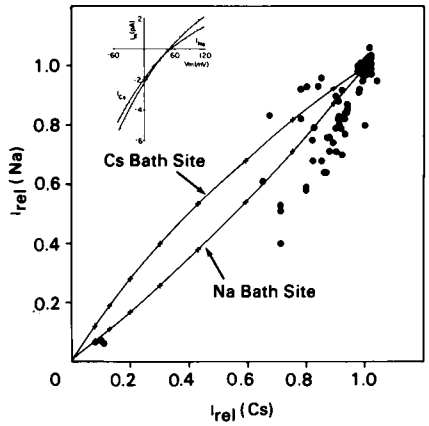

FIGURE 6 The current carried by Na at +200 mV relative to standard channel current (4.4 pA) is plotted against the current carried by Cs^+ at −120 mV relative to standard channel current (10.3 pA) for a group of channels observed in several bilayers. The solid curve shows the predictions of the three-barrier, two-site model where the well depth parameters for Na^+ and Cs^+ are varied by equal amounts on the Na^+ bath side of the membrane (*top curve*) or the Cs^+ bath side (*bottom curve*). The parameters were taken from Urban et al. (1980). The plus marks on the solid curves mark 0.5 *RT* increments in the well depths. Deepening the Na^+ well more than the Cs^+ well on the Na bath side of the membrane causes greater asymmetry (I_{Cs}/I_{Na}). The inverse is true if the change is on the Cs bath side. The inset shows a typical standard channel I-V and a mini channel I-V. Note the similarity in the reversal potentials. Front compartment 1 M NaCl. Back compartment 1 M CsCl. GMO Hex (50 mg/ml), 23°C.

well-depth was changed, provided that the differential is great enough.

These modeling considerations suggest the simple qualitative analysis of isopotential currents illustrated in Fig. 6. Here the current carried from the front chamber by Na^+ (at 200 mV) is plotted against the current carried from the back chamber by Cs^+ (at −120 mV) for each of several channels. Two predictions of the three-barrier, two-site model are shown for comparison. One is the predicted current when wells are decreased to equal extents for the two permeant species on one side of the channel (e.g., nearest the chamber containing 1.0 M CsCl), the other is that expected for equal well deepenings on the opposite side. Points falling between the curves are ambiguous: they could result from greater Cs^+ well deepening on the Na^+ bath side or greater Na^+-well deepening on the Cs^+-bath side. Points that fall below the lower curve result from greater Na^+ well-deepening on either side. Those above the upper curve result from greater Cs^+ well-deepening on either side. Standard channels are seen to form a cluster of points in the upper right hand corner; other points represent mini channels. Most of the mini channels have a greater decrease in I_{Na} than I_{Cs}, suggesting a greater increase in the binding affinity of one site for sodium.

We have also measured single channel IVs for standard and mini channels under a variety of other bi-ionic conditions. The results for combinations of Cs^+, K^+, Na^+, Li^+, and NH_4^+ can be summarized as follows: (*a*) compared with standard channels, minis generally have decreased conductance for both types of cations, that is in both limbs of the bi-ionic IV; (*b*) the amount of decrease in the two limbs is generally similar; the Na^+/Cs^+ combination plotted in Fig. 6 displayed the greatest disparity in the reduction of the two limbs; and (*c*) the reversal potentials were always within a 5–10 mV range.

In contrast, Ag^+ and H^+ conductance in minis behaved differently. The Ag^+ conductance of minis was examined by studying mini IVs in Ag^+/Na^+ bi-ionic conditions. Minis were detected in the usual percentages based on their decreased conductance at voltages where Na^+ was the main charge carrier. As exemplified in the inset to Fig. 7, however, minis frequently had essentially normal conductance at voltages where Ag^+ was the charge carrier. The regularity of this effect in the mini population is shown in the body of Fig. 7 where the current carried by Ag^+ is plotted against the Na^+ mediated current for a group of standard and mini channels. The standard channels are indicated by the dashed enclosure. Mini channels, reduced by as much as half in I_{Na}, often have very little reduction in I_{Ag}. The result is that the IVs of minis usually merge with standard channel IVs in the Ag^+-limb rather than distinctly crossing over, as would be usually seen for the alkali metal cations and ammonium.

In H^+/Cs^+ bi-ionic conditions the anomaly is even more striking because most mini IVs neither cross over nor merge. Instead, as shown in the inset in Fig. 8, they appear

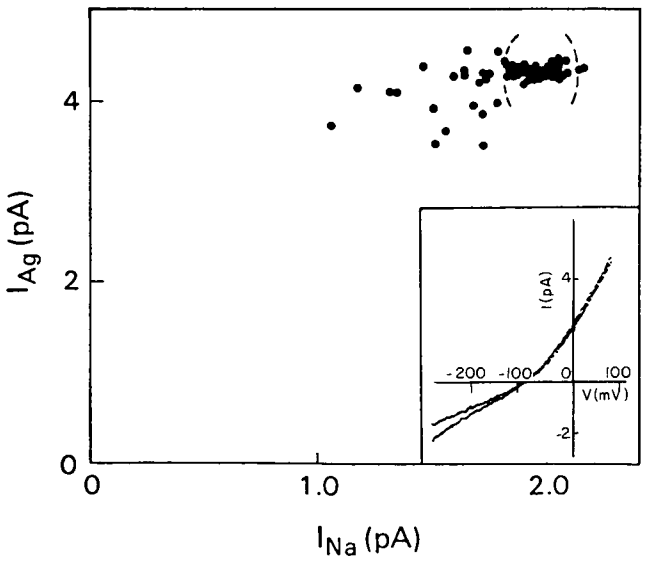

FIGURE 7 Ag^+-mediated current (at +60 mV) plotted against the absolute value of the Na^+-mediated current (at −250 mV) for each of a group of channels from several membranes. Standard channels are arbitrarily specified as those within the dashed enclosure. *Inset:* IV's of a typical standard channel (*open circles*) and a mini channel (*filled circles*). Front compartment 1.0 M AgF. Back compartment 0.49 M NaF, 0.01 M AgF. GMO Hex (50 mg/ml), 23°C.

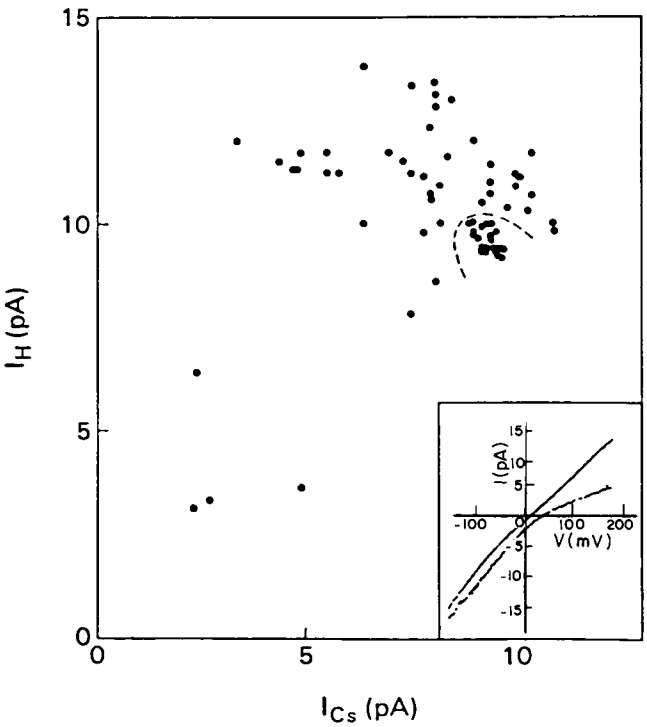

FIGURE 8 Absolute value of the H^+-mediated current (at −150 mV) is plotted against the Cs^+-mediated current (at +90 mV) for each of a group of standard and mini channels obtained from several different membranes. *Inset:* The IV for a typical standard channel (*open circles*) and mini channel (*filled circles*). Front compartment 1.0 M CsCl. Back compartment 0.1 M HCl. GMO/Hex (50 mg/ml), 23°C.

to be shifted. This is not a result of electrode potential drift because the mini IVs were stable over the several ramp cycles during the mini lifetime and they were usually bounded on both sides within seconds by standard channels which also had stable, unshifted IVs. We therefore conclude that mini channels actually have increased H^+ permeability, i.e., in H^+, minis are maxis. The body of Fig. 8 is a plot of I_H vs. I_{Cs} for a set of mini and standard channels. The standard channels are indicated by the dashed enclosure. It is evident that the bulk of the channels having reduced I_{Cs} conductance have increased I_H. We did find some channels which had large decreases both in I_{Cs} and I_H, but not as many as with decreased I_{Cs} and increased I_H. We also note that many of the channels which had normal I_{Cs} had increased I_H, suggesting that the H^+ conductance might detect conformational changes with more sensitivity than Cs^+ conductance.

The data in Fig. 8 imply that variant channels should have increased conductance in symmetrical HCl solution. Fig. 9 shows the single-channel current transition histogram obtained using symmetric 0.1 N HCl. Like the histograms for 1 M KCl, there is a sharp peak containing the majority of the channels. However, instead of the usual spread of minis, there are but 5% of the channels with conductances lower than the standard channels (<90 ps), while the majority of the variants (27%) appear distributed rather evenly above the conductance of the standard channels (110–200 pS). The sum of low conductance and high conductance variants constitute 31.6% of the transitions, typical of mini frequencies observed under other conditions (Busath and Szabo, 1988). Similar data were obtained in 0.001 N HCl, although the small conductances observed at this dilution (4.0 ± 0.2 ps for standard channels) rendered data analysis more difficult. Out of 418 transitions observed, 24 (5.7%) fell clearly below the main conductance peak (<3.8 ps) while 48 transitions (12%) fell clearly above it (>4.2 ps).

DISCUSSION

The observation that mini channel IVs are asymmetric in symmetric lipid membranes and bathing solutions indicates an asymmetry in the mini channel structure itself. The Eyring rate theory model provides a simple way to classify the degree of rectification and other aspects of the IV curvature. It is likely that the overall conclusions derived from a simple energy profile will continue to hold in more refined models as well. Increasing the strength of the *cis* binding site of the channel most readily generated the observed mini channel IV shapes. Barrier height changes produced IVs with inadequate rectification and inappropriate inflections. By our definition of *cis*, channels conduct better when net current flows into the *cis* side than when it flows out of the *cis* side. Thus, increased ion-binding affinity at the channel exit causes a greater reduction in current than increased affinity at the entrance. The computer simulations we performed indicate that this finding is generally expected for high ion concentrations for which current is largely exit-limited in the gramicidin channel. At lower concentrations, where current is entry-limited, changes in the channel entrance would have more significant effects.

Locating the well deeper in the channel seems to be the most reasonable secondary refinement. In the G_2, α_2 fit of the 23 mini channels in symmetrical 1 M KCl solutions, the best well position for each channel was correlated with the conductance decrease as shown in Fig. 10. This inward shift tends to improve the shape of the IV curve to better match the observed inflections.

Another likely secondary change was also considered: raising the barrier to entry and exit of the second ion on the side of the channel opposite to the modified well. The

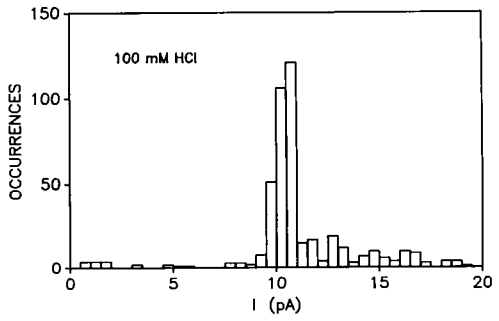

FIGURES 9 Histogram of proton conductance for gramicidin A channels in 0.1 M HCl. The potential across the membrane (GMO/HEX 50 mg/ml) was 100 mV so that 10 pA current transition corresponds to a 100 pS conductance transition. Note that minis are nearly absent (26 transitions smaller than 90 pA out of a total of 440 transitions, 5.9%). Also note the conspicuous presence of transitions larger than standard (113 transitions > 110 pS, 25.7%). There were 301 transitions in the standard range (90–110 pS), 68.4%. The total number of atypical transitions was 31.6%. T = 23°C.

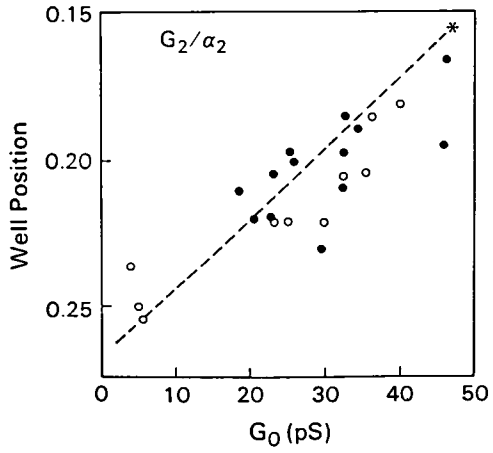

FIGURE 10 The optimal *cis* well position (α_2) for fitting the IV is plotted against the zero current conductance for each of the 23 mini channels. (*Filled circles*) $R < 1$; (*open circles*) $R > 1$. The asterisk represents the standard channels. 1 M KCl. GMO Hex (50 mg/ml), 23°C.

results of this fit are displayed in Fig. 11. The change in opposite barrier height is plotted against the well depth in the (G_2, ΔG_5) fit. Interestingly, the increase in the second-ion barrier equals the well deepening. We call this the plug-coupling fit and refer to the increase in opposite second-ion barrier height as the coupling energy. We chose this term to contrast a related concept, the repulsion energy. The second-ion barrier is often considered to differ from the entry barrier of an empty channel because of the electrostatic repulsion between two ions in a channel (e.g., Hille and Schwartz, 1978). We propose here that it could also differ because of energetic limitations on uncoupled motions of the two cations. If the increased depth of the abnormal well immobilizes the ion bound there and, because of the single file nature of the pore, also immobilizes the water molecules between the bound ion and the opposite pore mouth, the entry and exit of the second ion would be strongly hindered. With an ion bound in the abnormal site, immobilization of the ion and the adjacent solvent plug in the pore may increase the barrier to the entry of the second ion. Likewise, a second ion bound in the normal site would be less likely to exit because of the water plug connecting it to the more tightly bound ion. The movements of two ions in a pore would be coupled by the plug of water between them. This prediction should be accessible to molecular dynamic calculations.

Our observation of an increased well depth leads us to conclude that mini channels are caused by an increase in the ion binding strength at one of the cation binding sites

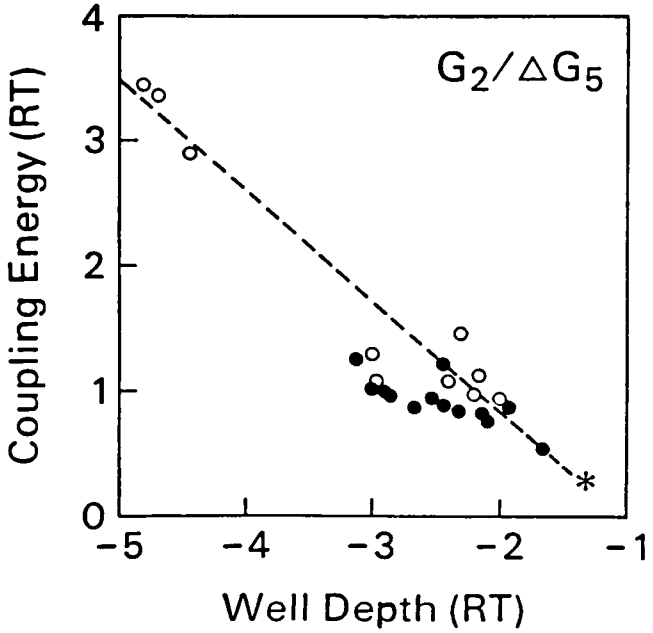

FIGURE 11 Correlation between coupling energy and well depth. Best fitting coupling energy (ΔG_5) is plotted against best fitting *cis* well depth for each of the 23 mini channels analyzed. Filled circles show data for channels with $R < 1$; open circles: $R > 1$. The asterisk shows the standard channel parameters from Table I. See text for explanation of the term "coupling energy."

present near each opening of the channel. Nuclear Magnetic Resonance measurements reported by Urry et al. (1982) indicate that these binding sites are formed by carbonyl oxygens of the peptide backbone and that the carbonyls of Trp-11 and Trp-13 are most perturbed by ion binding. It is therefore likely that atypical channels result from a conformational change in the vicinity of these carbonyls.

The Eisenman theory for ion selectivity (Eisenman, 1983) seems to describe the pattern of binding strength changes in minis. According to this electrostatic theory, increased binding site field strength should yield a greater increase in site affinity for Na^+ than Cs^+. We found that the sodium conductance is reduced more than the cesium conductance in 90% of the minis we observed (Fig. 6). Thus bi-ionic IV's are consistent with an increased binding affinity at one side of the pore.

Single-channel reversal potentials (V_{rev}) using alkali metal cations were similar for minis and standards. This finding can be used to argue in favor of an increased binding affinity as opposed to an increased barrier height. The energetic consequences of the channel modification are likely to differ for different ions. In the simplest permeation models (Independence Principle or single-occupancy) differential affinity changes do not affect the reversal potential but differential barrier height changes do (Hille, 1975). In multi-occupancy channels like gramicidin, differential affinity changes cause small reversal potential changes (Kohler and Heckmann, 1980) like those we observed with minis, but not the large changes predicted by differential barrier height changes.

Binding affinity at carbonyl oxygens 11 and 13 could be increased by (*a*) local narrowing of the pore, bringing carbonyl oxygens together in closer proximity (*b*) increased peptide backbone flexibility allowing local narrowing in response to cation occupancy, (*c*) increased carbonyl oxygen electronegativity resulting, for example, from changes in side chain electron-withdrawing, or (*d*) a change in electrostatic potential in the channel produced by distant changes, for example, side-chain dipoles. The increased H^+ conductance of minis rules out the long-range electrostatic field effect (*d*). It also rules out the theory that minis result from the binding of a charged ligand near the channel entrance. An externally induced electric field should affect H^+ in the same way as any other monovalent cation. The finding that minis have little or no decrease in silver conductance argues in favor of a local change in binding geometry (mechanisms a and b rather than c or d) which does not affect binding of the highly polarizable silver ion, but does increase binding of the less deformable alkali metal cations.[2] This conclusion must be

[2]As noted above for the example of Na/Cs biionic IV's, a deepened well for either ion causes a decreased current-limb for that ion. Therefore the lack of a decreased current limb for Ag in minis implies an unaffected Ag-binding affinity.

mitigated, however, by the finding that ammonium, with a broadly distributed positive charge, behaves like alkali metal cations rather than Ag^+ as far as mini channel IV's are concerned.

We suggest that H^+ conductance is affected by a different mechanism. Hydrogen enjoys a very high mobility in the gramicidin channel indicating that the Grotthuss mechanism is operative for H^+ transport (Hladky and Haydon, 1972). In bulk water, this mechanism involves the interchange of covalent and hydrogen bonds between O and H, allowing H^+ diffusion by way of electron motions rather than proton motions. The rate of diffusion is limited by the speed at which the newly formed hydronium ion forms hydrogen bonds for the next interchange (Conway et al., 1956). In ice, the water molecules are well oriented for the bond exchange and the H^+ mobility is much higher than in water (Conway and Bockris, 1958). In the gramicidin channel the waters are probably aligned favorably, as in ice, facilitating Grotthuss conductance (e.g., Mackay et al., 1984). We suggest that in mini channels, the modified binding site may enhance alignment of the water molecules, perhaps through increased hydrogen bonds to the carbonyl oxygens, resulting in an enhancement of the usual Grotthuss mechanism. Thus in minis the normal cation transport mechanism is inhibited by the enhanced binding, but their hydrogen transport is increased by the enhanced Grotthuss effect. In summary, the data presented here are best explained by a conformational alteration near the gramicidin channel mouth, resulting in an increased binding site affinity which includes a modification in the positions of the carbonyls in the channel interior and which enhances hydrogen bond alignment among the water molecules in the channel.

We wish to thank Lynnette Morgan, Pat Moreno, and Valerie Burrage for secretarial help and Greg Hemsley for experimental assistance, Drs. Don McBride, Ron Waldbillig, and Olaf Andersen contributed many helpful conversations.

This work was supported by National Institutes of Health grants GM26897, GM33361, and HL24820.

Received for publication 8 August 1987 and in final form 30 November 1987.

REFERENCES

Andersen, O. S. and J. Procopio. 1980. Ion movement through a gramicidin A channel. *Acta. Physiologica Scandinavia* Suppl. 481:27–35.

Andersen, O. S. 1983. Ion movement through gramicidin A channels. Single-channel measurements at very high potentials. *Biophys. J.* 41:119–133.

Begenisich, T. and M. Cahalan. 1980. Sodium channel permeation in squid axons. I. Reversal potential experiments. *J. Physiol. (Lond.).* 307:217–242.

Bevington, P. R. 1969. Data reduction and error analysis for the physical sciences. McGraw-Hill Book Company. New York.

Busath, D. and G. Szabo. 1988. Low conductance gramicidin A channels are head-to-head dimers of β^6-helices. *Biophys. J.* 689–695.

Conway, B. E., J. O'M Bockris and H. Linton. 1956. Proton conductance and the existence of H_3O ion. *J. Chem. Phys.* 24:834–850.

Conway, B. E. and J. O'M. Bockris. 1958. Proton conductance in ice. *J. Chem. Phys.* 28:354–355.

Eisenman, G., J. Sandblom and E. Neher. 1978. Interactions in cation permeation through the gramicidin channel. Cs, Rb, K, Na, Li, Tl, H and effects of anion binding. *Biophys. J.* 22:307–340.

Eisenman, G. 1983. The molecular basis of ionic selectivity in macroscopic systems. *In* Mass Transfer and Kinetics of Ion Exchange. L. Liberti and F. G. Helfferich, eds. NATO ASI Series. Martinus Nijhoff Pub., The Hague, 121–155.

Eisenman, G. and J. P. Sandblom. 1983. Energy barriers in ionic channels: data for gramacidin A interpreted using a single-file (3B4S") model having 3 barriers separating 4 sites. Physical chemistry of transmembrane ion motions. G. Spach, editor. Elsevier/North Holland Biomedical Press, Amsterdam. 329–348.

Eyring, H., R. Lumry and J. W. Woodbury. 1949. Some appliations of modern rate theory to physiological systems. *Rec. Chem. Prog.* 10:100–114.

Hille, B. 1975. Ionic selectivity of Na and K channels of nerve membranes. In membranes: A series of advances. G. Eisenman, ed. Marcel Dekker, Inc., New York. 3:255–323.

Hille, B. and W. Schwarz. 1978. Potassium channels as multi-ion single-file pores. *J. Gen. Physiol.* 72:409–442.

Hladky, S. B. and D. A. Haydon. 1972. Ion transfer across lipid membranes in the presence of gramicidin A. I. Studies of the unit conductance channel. *Biochim. Biophys. Acta.* 274:294–312.

Kohler, H.-H. and K. Heckmann. 1980. The relation between binding affinity and selectivity of a pore. *J. Membr. Sci.* 6:45–59.

Levitt, D. G., S. R. Elias, and J. M. Hautman. 1978. Number of water molecules coupled to the transport of sodium potassium, and hydrogen ions via gramicidin, nonactin, or valinomycin. *Biochim. Biophys. Acta.* 512:436–451.

Mackay, D. H. J., P. H. Berens, and K. R. Wilson. 1984. Structure and dynamics of ion transport through gramicidin A. *Biophys. J.* 46:229–248.

McBride, D. W. 1981. Anomalous mole fraction behavior, momentary block, and lifetimes of gramicidin A in silver and potassium fluoride solutions. Ph.D. Thesis, Univ. of California, Los Angeles.

Monoi, H. and H. Uedaira, 1979. Na^+ interacting with gramicidin D. A nuclear magnetic resonance study. *Biophys. J.* 25:535–540.

Robinson, R. A. and R. H. Stokes. Electrolyte Solutions. Butterworth, London. 1965.

Rosenberg, P. A. and A. Finkelstein. 1978. Interaction of ions and water in gramicidin A channels. Streaming potential across lipid bilayer membranes. *J. Gen. Physiol.* 72:327–340.

Sandblom, J., G. Eisenman, and E. Neher. 1977. Ionic selectivity, saturation, and block in gramicidin A channels: I. Theory for the electrical properties of ion selective channels having two pairs of binding sites and multiple conductance states. *J. Membr. Biol.* 31:383–417.

Shagina, L. V., A. E. Grinfeldt, and A. A. Lev. 1978. Interaction of cation fluxes in gramicidin A channels in lipid bilayer membranes. *Nature (Lond.).* 273:243–245.

Urban, B. W., S. B. Hladky, and D. A. Haydon. 1978. The kinetics of ion movements in the gramicidin channel. *Fed. Proc.* 37:2628–2632.

Urban, B. W. and S. B. Hladky. 1979. Ion transport in the simplest single file pore. *Biochim. Biophys. Acta.* 554:410–429.

Urban, B. W., S. B. Hladky and D. A. Haydon. 1980. Ion movements in

gramicidin pores. An example of single file transport. *Biochim. Biophys. Acta.* 602:331–354.

Urry, D. W., C. M. Venkatachalam, A. Spisni, R.J. Bradley, T. L. Trapane and K. U. Prasad. 1980. The malonyl gramicidin channel: NMR-derived rate constants and comparisons of calculated and experimental single-channel currents. *J. Membr. Biol.* 55:29–51.

Urry, D. W., K. U. Prasad, and T. L. Trapane. 1982. Location of monovalent cation binding sites in the gramicidin channel. *Proc. Natl. Acad. Sci. USA.* 79:390–394.

Woodbury, J. W. 1971. Eyring rate theory model of the current-voltage relationships of ion channels in excitable membranes. In Channel Dynamics: Papers in Honor of Henry Eyring. J. O. Hirschfelder, editor. John Wiley and Sons, Inc. New York. 601–617.